Electronic structure of pure and alkali-metal-intercalated VSe_2

H. E. Brauer and H. I. Starnberg
Department of Physics, Chalmers University of Technology and Göteborg University, SE-412 96 Göteborg, Sweden

L. J. Holleboom
Department of Theoretical Physics, University of Lund, SE-223 62 Lund, Sweden

V. N. Strocov
Institute for High-Performance Computations and Data Bases, P.O. Box 76, 194291 St. Petersburg, Russia

H. P. Hughes
Cavendish Laboratory, Madingley Road, Cambridge CB3 0HE, United Kingdom
(Received 10 April 1998)

The valence bands of the layered compound VSe_2 and the related intercalation compounds Na_xVSe_2, K_xVSe_2, and Cs_xVSe_2 have been investigated by means of angle-resolved photoelectron spectroscopy, and compared to self-consistent linear augmented plane-wave (LAPW) band calculations. The intercalation compounds were prepared *in situ* by deposition of Na, K, and Cs on VSe_2 cleavage surfaces. The intercalation was monitored by core-level spectroscopy, and although K was found to intercalate more slowly than Na and Cs, estimated alkali concentrations of $x=0.2-0.3$ were reached for all three alkali metals. Additional depositions mainly seemed to increase the intercalation depth. Good agreement between LAPW calculations and valence-band spectra was found, in particular for the dispersion along the layers. Normal-emission spectra, obtained at different photon energies, indicated vanishing perpendicular dispersion, but in spectra measured under variation of the emission angle some band-edge signatures were seen, which suggests that some perpendicular dispersion remains, in accordance with the LAPW calculations. The lack of dispersion in the normal-emission spectra could be due to intercalation induced structural transformations, leading to stacking disorder. Also correlation effects may contribute. The rigid-band model is found inadequate, except as a crude approximation, for describing the changes during the initial phase of intercalation. It might be used to describe the continued intercalation, however, under condition that the intercalation modified bands are used. The need for studies that probe both electronic and crystallographic structure (including defects) is stressed. [S0163-1829(98)08536-1]

I. INTRODUCTION

Layered transition metal dichalcogenides (TMDC's) are highly anisotropic materials with a multitude of interesting properties, often regarded as prototypes of two-dimensional (2D) materials. Each layer consists of a hexagonal transition metal sheet sandwiched between two similar chalcogen sheets. The interaction between adjacent layers is weak and van der Waals-like. Many distinct TMDC polytypes are found, with differences in the intralayer coordination of the metal and in the stacking of the layers. Periodic lattice distortions (PLD's) and associated charge density waves (CDW's) are frequently observed.[1]

Of particular interest is the ability of TMDC's to form intercalation complexes, with foreign atoms or molecules introduced into the van der Waals gaps between the layers.[2,3] The intercalation of TMDC's is usually associated with transfer of electrons from the intercalant to the host layers, and this charge transfer is indeed considered to drive the intercalation process. The intercalation-induced changes are often described in terms of the rigid-band model (RBM), in which it is assumed that the electronic band structure of the host lattice remains basically unchanged, with only the band filling being altered by the charge transfer. However, intercalation with species larger than the available interstitial sites will affect the degree of anisotropy, since an increase of the interlayer separation is then inevitable. As a consequence, one may then expect changes not compatible with the RBM.

In earlier investigations of intercalation complexes, these were produced by methods not compatible with ultrahigh-vacuum conditions. More recently, intercalation has been shown to occur spontaneously as suitable intercalants are UHV deposited *in situ* onto clean surfaces of many TMDC's. Such systems are well suited for studies by means of surface science techniques, such as photoelectron spectroscopy (PES) or inverse photoelectron spectroscopy (IPES). Particularly valuable is the possibility to follow closely the changes in the electronic structure at any stage of the intercalation process. So far, most PES studies of *in situ* intercalated TMDC's have been done with noble metals[4–8] or alkali metals[9–28] as intercalants. By exploiting the angular dependence in PES, it is possible to map the valence bands in detail,[15,19,21,22,24,25] and to compare with calculated bands of intercalated TMDC's.

Among the most studied TMDC's is VSe_2, which adopts the $1T$ structure, characterized by octahedral coordination of the metal and layers stacked without lateral displacement as illustrated in Fig. 1. VSe_2 is metallic due to a half-filled band

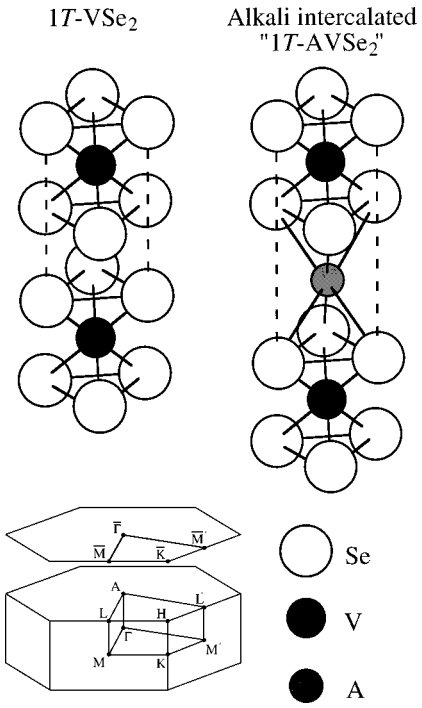

FIG. 1. Crystallographic structure of $1T$-VSe_2 and the assumed $1T$ structure of alkali-metal-intercalated VSe_2. A=Na, K, or Cs. The corresponding surface and bulk Brillouin zones are shown in the lower left corner.

of V $3d$ character, and its band structure has been well characterized using PES and IPES,[29–34] and found to agree fairly well with calculations.[35–37] VSe_2 exhibits a (4×4) CDW/PLD below 112 K, which is much weaker than for other group V $1T$ polytypes. This and other anomalies are attributed to the V $3d$ band being very narrow.[2,3]

As a step toward better understanding of the properties of alkali-metal-intercalated TMDC's, and of the mechanisms behind *in situ* intercalation, here we report self-consistent band-structure calculations for VSe_2 and for the hypothetical compounds $NaVSe_2$, $KVSe_2$, and $CsVSe_2$, together with angle-resolved photoemission results from VSe_2, before and after *in situ* intercalation with Na, K, and Cs.

II. BAND-STRUCTURE CALCULATIONS

A. Method and crystal structures

Self-consistent scalar-relativistic[38] band-structure calculations of VSe_2 and the hypothetical compounds $NaVSe_2$, $KVSe_2$, and $CsVSe_2$ were obtained by applying the linear augmented plane-wave (LAPW) method within the local-density approximation of density-functional theory. The calculations used 65 **k** points in the irreducible part of the Brillouin zone (BZ) together with 400 LAPW basis functions. The parametrized Ceperley-Alder[39] form of the exchange-correlation potential was used. There were no restrictions on the potential, i.e., the calculations were of so-called full potential type, which is important in such highly anisotropic structures as studied here.

In order to limit the calculational efforts, the intercalated alkali atoms were assumed to occupy octahedral sites between the VSe_2 layers, as shown in Fig. 1, thus retaining the $1T$ structure. The structural parameters used in the calculations for VSe_2 were 3.35 and 6.12 Å for the in-plane (a axis) and interlayer (c axis) lattice parameters, respectively.[1] Regarding the alkali-metal-intercalated compounds, the in-plane lattice parameter was increased to 3.58 Å for all three compounds, while the interlayer lattice parameters were increased to 6.70 Å ($NaVSe_2$), 7.77 Å ($KVSe_2$), and 8.70 Å ($CsVSe_2$). These estimates were based on comparisons with other alkali-metal intercalates[2,3,40] and ionic radii considerations.[41] Also shown in Fig. 1 are the corresponding bulk and surface BZ's.

B. VSe_2

Figure 2(a) presents the LAPW band structure of VSe_2: At (and above) the Fermi energy E_F five conduction bands[42] derived mainly from V $3d$ orbitals, and below E_F six valence bands primarily of Se $4p$ character. Two Se $4s$ bands about 14 eV below E_F are not included in the figure. Between the V $3d$ conduction bands and the higher conduction bands (not shown) is a fundamental gap of more than 1.5 eV. With a work function of 5.76 eV for VSe_2,[31] the vacuum level is found just above the upper edge of this gap, which induces image potential states,[31] and has a profound influence on the electron emission properties of VSe_2.[43] The calculated occupied width of the lowest conduction band, of d_{z^2} character, is 0.8 eV, about twice as much as found experimentally.[29,30] Near Γ the distinction between valence and conduction bands is somewhat blurred, as the V $3d_{z^2}$ band overlaps with the uppermost Se $4p$ bands.

The present band-structure calculation shows an overall qualitative agreement with earlier calculations,[35–37] but is the only one to predict a direct, although very small (21 meV), overlap between the valence and conduction bands at the zone center. Such an overlap was inferred by the high-resolution photoemission study of Ref. 30, although the hole surface at the zone center, indicated in that study, is not reproduced by the calculation.

C. $NaVSe_2$, $KVSe_2$, and $CsVSe_2$

Figures 2(b)–2(d) show the calculated band structures for the hypothetical alkali intercalation compounds. The V $3d$-derived conduction bands are altered for all three compounds by hybridization with alkali $3s$, $4s$, or $6s$ bands, respectively, which may cancel the fundamental band gap of pure VSe_2. This clearly happens for $CsVSe_2$, which displays a wealth of higher bands, with additional contributions from empty Cs $4f$ and $5d$ states. Of the $NaVSe_2$ and $KVSe_2$ conduction bands, only the three lowest are shown. The Se $4s$ bands, which are excluded also from Figs. 2(b)–2(d), are not much affected by the intercalation, but for $CsVSe_2$ three Cs $5p$-derived bands are found just a few eV higher in energy. Some characteristics of the LAPW band structures are summarized in Table I.

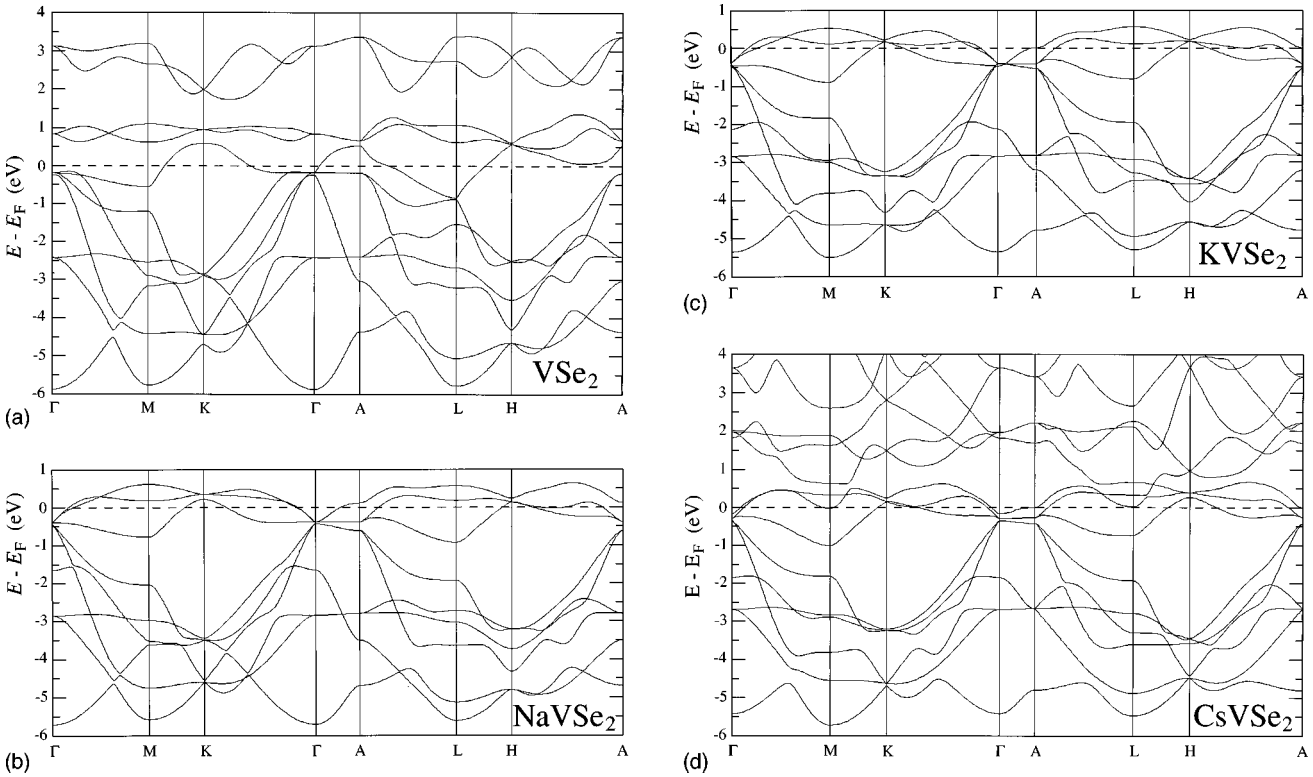

FIG. 2. Calculated LAPW band structures of (a) VSe_2, (b) $NaVSe_2$, (c) $KVSe_2$, and (d) $CsVSe_2$.

III. EXPERIMENTAL DETAILS

Two different experimental systems were used for recording the photoelectron spectra. The first one, with a base pressure typically 8×10^{-11} torr, is equipped with a rare gas discharge lamp providing unpolarized He I radiation ($h\nu = 21.22$ eV). The other system, with base pressure about 2×10^{-10} torr, utilizes synchrotron radiation from beamline 41 at the MAX I storage ring in Lund, Sweden. The beamline incorporates a toroidal grating monochromator providing photons with energies in the range 15–200 eV and polarization in the plane of incidence. The incidence angle of the incoming light φ was kept at 45° in both experimental systems. Both electron energy analysers have $\pm2°$ angular acceptance, and in both systems the total energy resolution was typically 0.1 eV. Both systems are equipped with low-energy electron-diffraction (LEED) optics.

TABLE I. Calculated band-structure characteristics of pure and alkali-metal-intercalated VSe_2. All entries are binding energies (relative to E_F) in eV. Values for the highest and lowest Se 4p bands at each symmetry point are separated by a slash.

		VSe_2	$NaVSe_2$	$KVSe_2$	$CsVSe_2$
V 3d	M	0.6	0.8	0.9	1.0
	L	0.8	0.9	0.8	0.8
Se 4p	Γ	0.1/5.9	0.5/5.7	0.4/5.3	0.4/5.4
	A	0.1/4.4	0.6/4.7	0.5/4.8	0.4/4.8
	M	1.2/5.8	2.0/5.6	1.8/5.5	1.9/5.7
	L	0.9/5.8	1.9/5.6	2.0/5.3	1.9/5.5
	K	2.9/4.7	3.4/4.6	3.2/4.6	3.2/4.7
	H	2.5/4.7	3.2/4.8	3.4/4.6	3.4/4.5
Se 4s		12.5/14.7	---	---	12.9/14.5

The VSe_2 single crystals were attached to the sample holder by silver-filled epoxy resin. Clean mirrorlike (0001) surfaces were obtained by cleavage *in situ*. The samples were azimuthally oriented in the $\bar{\Gamma}\bar{K}$ and $\bar{\Gamma}\bar{M}$ azimuths by LEED, which showed sharp hexagonal 1×1 spots with low background, confirming the high quality of the surfaces. The inequivalent $\bar{\Gamma}\bar{M}$ and $\bar{\Gamma}\bar{M}'$ crystallographic directions were identified as described in Ref. 32. The samples were kept at room temperature at all times. Na, K, and Cs were deposited from carefully outgassed getter sources (SAES) positioned about 15 mm in front of the samples. They were operated at constant current (different for different alkali sources) for a certain time, typically 2–5 min. The alkali metal started to evaporate about 45 s after the current was switched on. The amount of alkali metal deposited depends strongly on the evaporation conditions, but we estimate that far more alkali metal was deposited than required to obtain monolayer coverage. The deposition and intercalation process was monitored by recording alkali-metal core-level spectra (Na 2p, K 3p, and Cs 4d). Valence-band and core-level spectra (Se 3d and V 3p) were recorded for both pure and alkali-metal-intercalated VSe_2.

The clean (0001) surface of VSe_2 is known to be chemically very inert due to the absence of dangling bonds, but the alkali-metal-intercalated surfaces turned out to be remarkably inert as well. Core-level and valence-band spectra indicated only moderate contamination, and showed no significant surface degrading during time intervals extending up to

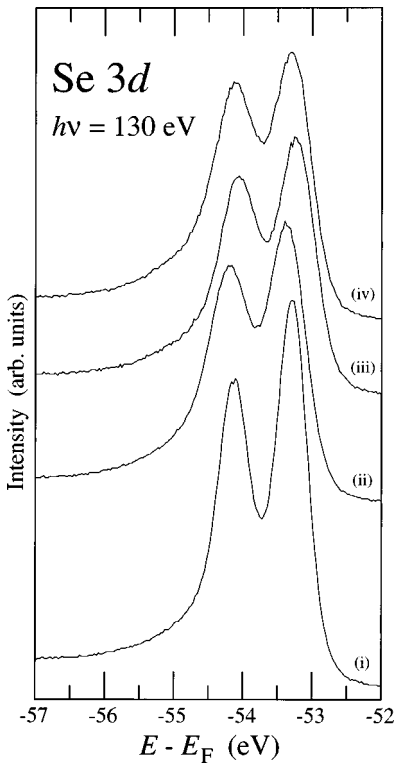

FIG. 3. Se $3d$ core-level spectra recorded with $h\nu=130$ eV and $\theta=0°$ for VSe_2 and after deposition of Na. Elapsed time after the first Na deposition is denoted by *t*. Spectrum (*i*) is from VSe_2, (*ii*) after one Na deposition ($t=0$ h), (*iii*) after one deposition ($t=6.5$ h), and (*iv*) after a second Na deposition ($t=17.5$ h).

48 h after the initial alkali-metal deposition. This inertness is probably due to the fact that no metallic alkali overlayer is formed at room temperature. The LEED pattern remained sharp but fainter after intercalation. The background intensity increased, but no superlattice spots were seen.

IV. EXPERIMENTAL RESULTS

A. Core levels

Figure 3 shows Se $3d$ core-level spectra recorded (i) from the clean VSe_2 surface, (ii) immediately after the first Na deposition (2 min, 6.0 A), (iii) 6 h later, and (iv) after a second Na deposition (2 min, 6.0 A) 17 h after the initial one. The spectra were measured normal to the surface ($\theta=0°$) with $h\nu=130$ eV. Se $3d$ spectra obtained after K and Cs depositions are not shown, as the results were not significantly different from those obtained with Na.

Figure 4(a) presents Na $2p$ spectra recorded with $h\nu=82$ eV after Na deposition. Spectrum (*i*) was recorded with $\theta=0°$ immediately after the first Na deposition (2 min, 6.0 A). One strong peak, labeled *I*, appears at 30.7-eV binding energy (BE) together with a weak structure *S* at 31.8-eV BE. Spectrum (*ii*) was recorded 0.5 h later, with $\theta=75°$, to enhance the surface sensitivity. In spectrum (*iii*), which was recorded 13 h after the deposition, again with $\theta=75°$, peak *I* remains at 30.7-eV BE, but peak *S* has shifted to 31.4-eV BE. In spectrum (*iv*), which was recorded with $\theta=0°$ immediately after the second Na deposition (17 h after the initial one), the BE of peak *S* is still reduced, but the spectrum is otherwise very similar to the initial one.

Spectra of the K $3p$ core level recorded with $h\nu=33$ eV after repeated K depositions are shown in Fig. 4(b). Again two peaks, *I* and *S*, are observed, but in contrast to the Na results, peak *S* is here the dominant feature. Spectra (*i*), (*ii*), and (*iii*) were recorded after one, three, and five depositions, respectively. The magnitude of each deposition was successively increased, going from 2 min at 5.0 A for the first deposition to 5 min at 5.3 A for the fifth deposition. The elapsed time between the first and fifth depositions was 7.5 h. Peak *I* is gaining in intensity for each K deposition, but remains at 17.4-eV BE, while peak *S* has almost constant intensity but gradually shifts from 19.0 to 18.4 eV.

Figure 4(c) shows Cs $4d$ spectra during the course of Cs deposition. The spectra were recorded with $h\nu=100$ eV (using second-order grating diffraction). After an initial deposition (5 min, 5.0 A) four conspicuous peaks appear, as seen in spectrum (*i*). The Cs $4d$ level is a doublet with 2.3-eV spin-orbit splitting, and the $4d_{3/2}$ and $4d_{5/2}$ components, are further split into two peaks each, corresponding to chemically different forms of Cs. In analogy with the Na $2p$ and K $3p$ cases, we label the $4d_{5/2}$ peaks I_1 and S_1, and the $4d_{3/2}$ peaks I_2 and S_2. Spectra (*ii*) and (*iii*) were recorded after two and ten depositions, respectively. Going from one to ten depositions I_1 (I_2) only shifts slightly downwards, from 75.7 (78.0) to 75.8 (78.1) BE, while S_1 (S_2) shifts markedly upwards, from 76.9 (79.2) to 76.4 (78.7) BE.

The Se $4s$ bands, located approximately 14 eV below the Fermi level, are usually considered as ''semicore'' levels, despite the fact that band calculations predict significant dispersion. The very small photoexcitation cross section of these levels can be enhanced by lowering the photon energy, but then problems arise due to the inelastic background, which becomes very intense and uneven at low kinetic energy. The background variations can be largely eliminated, however, by measuring in the constant-final-state (CFS) mode, in which the emission angle and the kinetic energy is kept constant while scanning the photon energy. Such CFS spectra from VSe_2 and Cs_xVSe_2, with $E_{kin}=6.0$ eV, are shown in Fig. 5(a): (*i*) for VSe_2 with $\theta=60°$ (probing along the *ML* line), (*ii*) for VSe_2 with $\theta=0°$ (probing along the ΓA line), and (*iii*) for Cs_xVSe_2 with $\theta=0°$ (also along the ΓA line). The latter spectrum also contains a contribution from the Cs $5p$ levels, but these features are also easily observable in the ordinary energy distribution curve (EDC) mode. To illustrate the usefulness of the CFS, mode, Fig. 5(b) shows the Se $4s$ and Cs $5p$ CFS spectra from Fig. 5(a) together with a corresponding EDC.

Figure 5(c) shows the V $3p$ core-level spectrum obtained from clean VSe_2. It is extremely broad and distorted (due to rapid super-Coster-Kronig core-hole decay), which hinders the extraction of useful information. This level is therefore not discussed in the following.

B. Valence bands

Extensive measurements of valence-band EDC's were performed on pure and alkali-metal-intercalated VSe_2, in order to map the band structure. Different series of EDC's were measured, either at normal emission with different photon energies (normal emission series), or with constant photon energy at different emission angles θ (angular series).

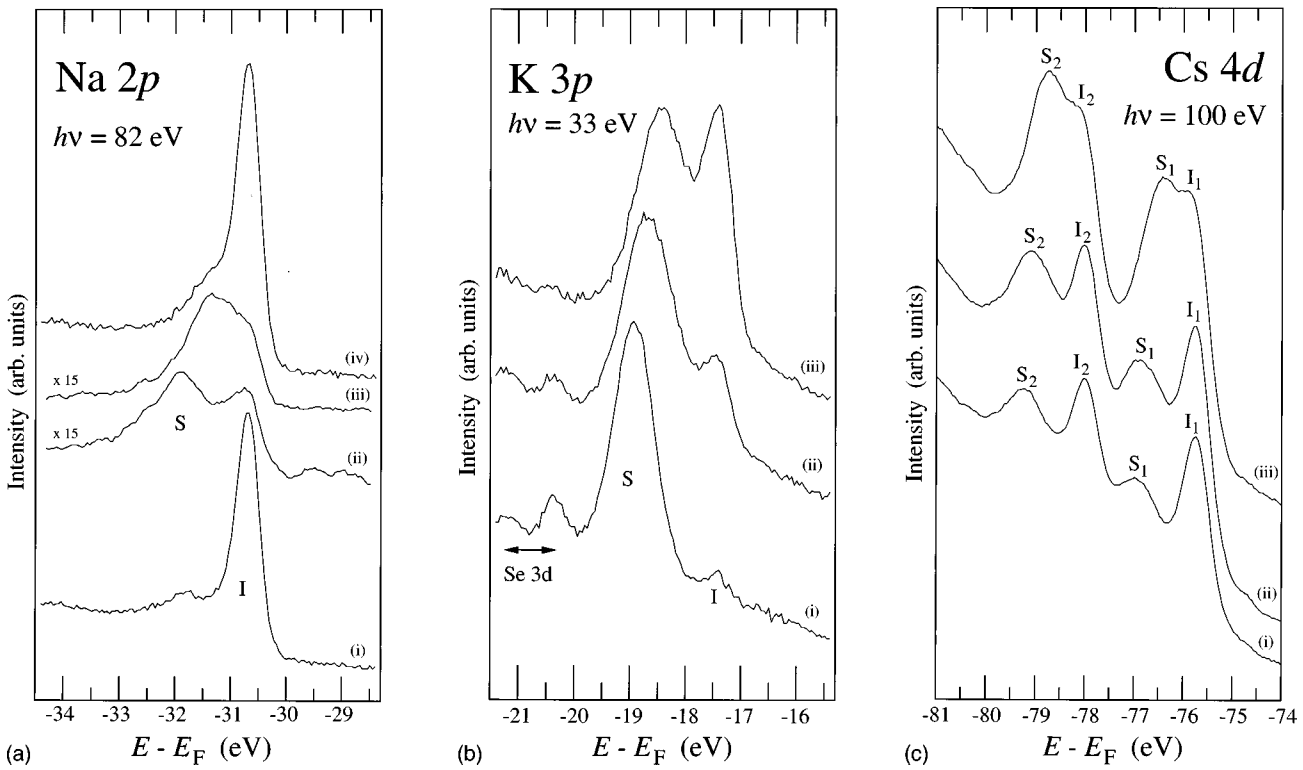

FIG. 4. (a) Na $2p$ core-level spectra with $h\nu=82$ eV ($\theta=0°$ unless noted) during the course of Na depositions. Spectrum (*i*) is recorded after one Na deposition ($t=0$ h), (*ii*) after one deposition but $\theta=75°$ ($t=0.5$ h), (*iii*) after one deposition but $\theta=75°$ ($t=13$ h), and (*iv*) after a second deposition ($t=17$ h). (b) K $3p$ core-level spectra with $h\nu=33$ eV ($\theta=0°$) during the course of K depositions. The Se $3d$ core level (excited by second order grating diffraction) is marked. Spectrum (*i*) is measured after one K deposition ($t=0$ h), (*ii*) after three depositions ($t=3$ h), and (*iii*) after five depositions ($t=7.5$ h). (c) Cs $4d$ core-level spectra with various amount of deposited Cs with $h\nu=100$ eV and $\theta=0°$. Spectra (*i*), (*ii*), and (*iii*) were recorded after one, two, and ten Cs depositions, respectively.

By applying a bias (-5.0 V) to the sample, the work function could be determined from the cutoff energy of the secondary electrons. We found $\Phi=5.7$ eV for the clean VSe_2, in good agreement with other measurements.[31] The work function of Cs_xVSe_2 was determined in the same way, and here we found $\Phi=3.5$ eV, i.e., a decrease by 2.2 eV.

Figure 6(a) presents normal-emission EDC's of VSe_2 with $h\nu=20-40$ eV. The strong and very sharp peak near E_F, arising from V $3d$ band states, dominates at all photon energies. The Se $4p$ band peaks are weaker in intensity and much broader, but several of the structures are seen to disperse as the photon energy is changed. Figures 6(b)–6(d) shows analogous normal-emission EDC's for Na_xVSe_2, K_xVSe_2, and Cs_xVSe_2. The spectra all show a strong nondispersive peak just below E_F, two or three minor peaks below it, and a relatively intense broad peak at the valence band bottom. For Na_xVSe_2 and K_xVSe_2 some slight dispersion is observed, e.g., for the broad peak, but for Cs_xVSe_2 no dispersion is seen within the experimental resolution. The K_xVSe_2 peaks are more broadened and less well defined than for the other systems.

Angular series of EDC's were recorded in the $\bar{\Gamma}\bar{K}$ and $\bar{\Gamma}\bar{M}(\bar{\Gamma}\bar{M}')$ azimuthal directions with $h\nu=21.22$ eV (He I line) and with $h\nu=14$, 24, 30, and 38 eV (synchrotron radiation). These EDC's are not explicitly shown here (but some of them have been published elsewhere[15]). Instead, the results of these measurements are condensed into structure plots, as described and discussed in Sec. V. Experimental band-structure characteristics, which were determined from these data, are summarized in Table II.

V. DISCUSSION

A. Intercalation process

Distinct chemically shifted alkali-metal core-level peaks are a common feature of alkali-metal/TMDC systems.[13,17–19,21,22,26–28] The peaks labelled I, I_1, and I_2 in Figs. 4(a)–4(c) are attributed to intercalated alkali-metal atoms, while the peaks S, S_1, and S_2 are associated with atoms on the surface. This identification is confirmed by the angular dependency of the relative intensities, as seen in Fig. 4(a) for the case of Na deposition: At normal emission peak I dominates, but at grazing emission ($\theta=75°$) peaks I and S becomes similar in magnitude, as the photoelectrons from intercalated Na are suppressed by the longer distance to travel before reaching the surface. In general, the intercalation peaks are more narrow than the surface-related peaks, which reflects the more well-defined chemical state of the intercalated alkali-metal atoms. As the charge balance between intercalant and host layers depends on the stoichiometry, the intercalation peaks may shift when more metal is deposited. Such effects are small, however, and we observed a slight ($\sim$0.1 eV) such shift only for the Cs_xVSe_2 system.

A comparison with previous alkali/TMDC studies suggests that the core-level BE's of intercalated alkali species are rather independent of the host material: For the Na $2p$

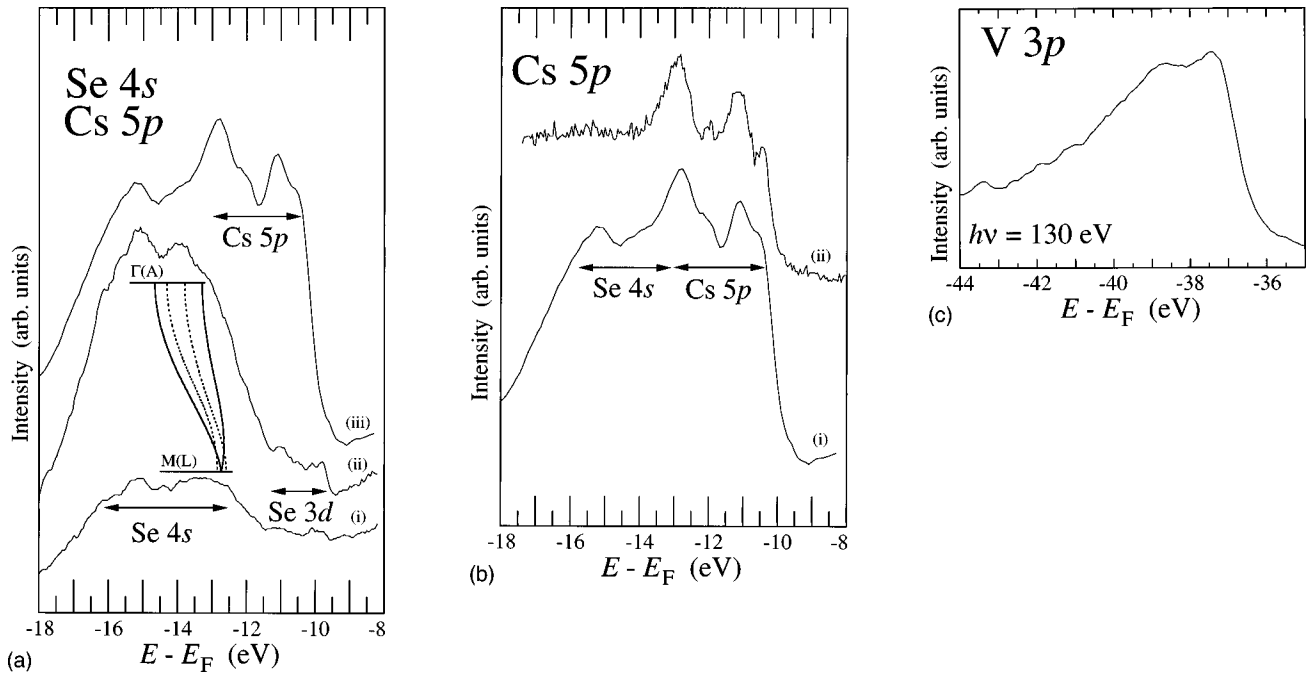

FIG. 5. (a) Se 4*s* spectra for VSe_2 and Cs_xVSe_2 measured in the CFS mode with $E_{kin}=6.0$ eV. Spectrum (*i*) is from VSe_2 with $\theta=60°$ (corresponding to $\bar{M}$), (*ii*) from VSe_2 but with $\theta=0°$ ($\bar{\Gamma}$), and (*iii*) from Cs_xVSe_2 (after four Cs depositions) with $\theta=0°$. The inset shows the calculated dispersion of the Se 4*s* bands along ΓM (full lines) and *AL* (dashed lines). A weak doublet structure due to Se 3*d* electrons, excited through second-order grating diffraction, is also indicated. (b) Cs 5*p* and Se 4*s* normal-emission spectra from Cs_xVSe_2 (after four Cs depositions) measured (*i*) in the CFS mode with $E_{kin}=6.0$ eV, and (*ii*) in the EDC mode with $h\nu=65$ eV. (c) V 3*p* core-level spectrum measured from VSe_2 with $h\nu=130$ eV and $\theta=0°$.

level we find good agreement with results from the Na/WSe_2 and Na/TaS_2 systems,[11,18] and for Cs 4*d* our BE's agree very well with those reported for Cs/TiS_2 and $Cs/ZrSe_2$.[21,22,28] For the K 3*p* level, however, we find a BE of 17.4 eV for the intercalation component, in contrast to 18.4 eV as reported for the K/WS_2 system.[9] As this latter value is close to our BE for the K 3*p* surface component, one may speculate that the peak reported for K/WS_2 was actually surface related.

In contrast to the intercalation peaks, the ones originating from surface alkali species depend significantly not only on the deposited amount of alkali metal, but also on the elapsed time. This is particularly evident in the Na 2*p* grazing emission spectra of Fig. 4(a): In spectrum (*ii*), soon after the initial deposition, the surface component *S* peaks at 31.9-eV BE, while in spectrum (*iii*), recorded 13 h later, the *S* peak appear shifted to 31.4-eV BE. Figures 4(b) and 4(c) show analogous shifts of the K and Cs surface components, although here the time dependence is not separated from the effect of repeated alkali depositions. A full understanding of the observed changes would require detailed knowledge of alkali adsorption sites on the VSe_2 surface, which is not yet available. Alkali-metal atoms are highly mobile on TMDC cleavage planes, and a recent study of the Cs/TiS_2 system has shown that several different alkali overlayer phases may exist, depending on temperature and coverage.[28] The absence of any extra LEED spots during the present study suggests that the alkali-metal atoms remaining on the VSe_2 surface are disordered at room temperature, occupying slightly inequivalent sites. Further adsorption sites may also be found at surface defects, such as steps, vacancies, and dislocations, where alkali-metal atoms could be quite firmly trapped, as these defects are presumably more reactive than the ideal cleavage planes. Contamination of the surface may introduce additional alkali adsorption sites, as well as modify the already existing sites. With this interpretation, the time-dependent shifts of surface core-level features simply reflect a redistribution of the surface alkali atoms, either by formation of new defect sites, or induced by surface contamination. During the intercalation reaction, the alkali atoms are believed to enter the interlayer gaps via crystal edges, surface steps, and other defects, from which they rapidly diffuse along the layers. As a frontline of diffusing atoms moves into previously unintercalated parts of the crystal, the layers are bent and wedged apart, which may cause them to break, whereby new defects are formed. Another type of structural change, which could be important in this context, concerns the stacking of the layers. Diffraction studies of powder samples have shown that the coordination of the intercalated alkali ions can be either octahedral or trigonal prismatic.[44–46] The obtained structure depends on the alkali concentration and ionic size (and also on the covalency of the host), but for the heavier alkalis (and for Na in moderate concentration) a 3*R* stacking with trigonal prismatic alkali coordination is generally expected. Such a stacking change is implied by the large increase ($\sim$1.6 Å) in the layer separation observed for the Na/VSe_2 system by scanning tunneling microscopy. During a $1T\rightarrow 3R$ transformation adjacent layers are required to slide relative to each other,[47] which could produce more defects, and also change the coordination of alkali atoms already trapped by defects. Stacking changes during *in situ* intercalation of large single crystals have not been studied so far, but as the sliding sheets are much larger than in powder samples, such stacking transformations will probably occur more slowly. Further investigations will hopefully resolve

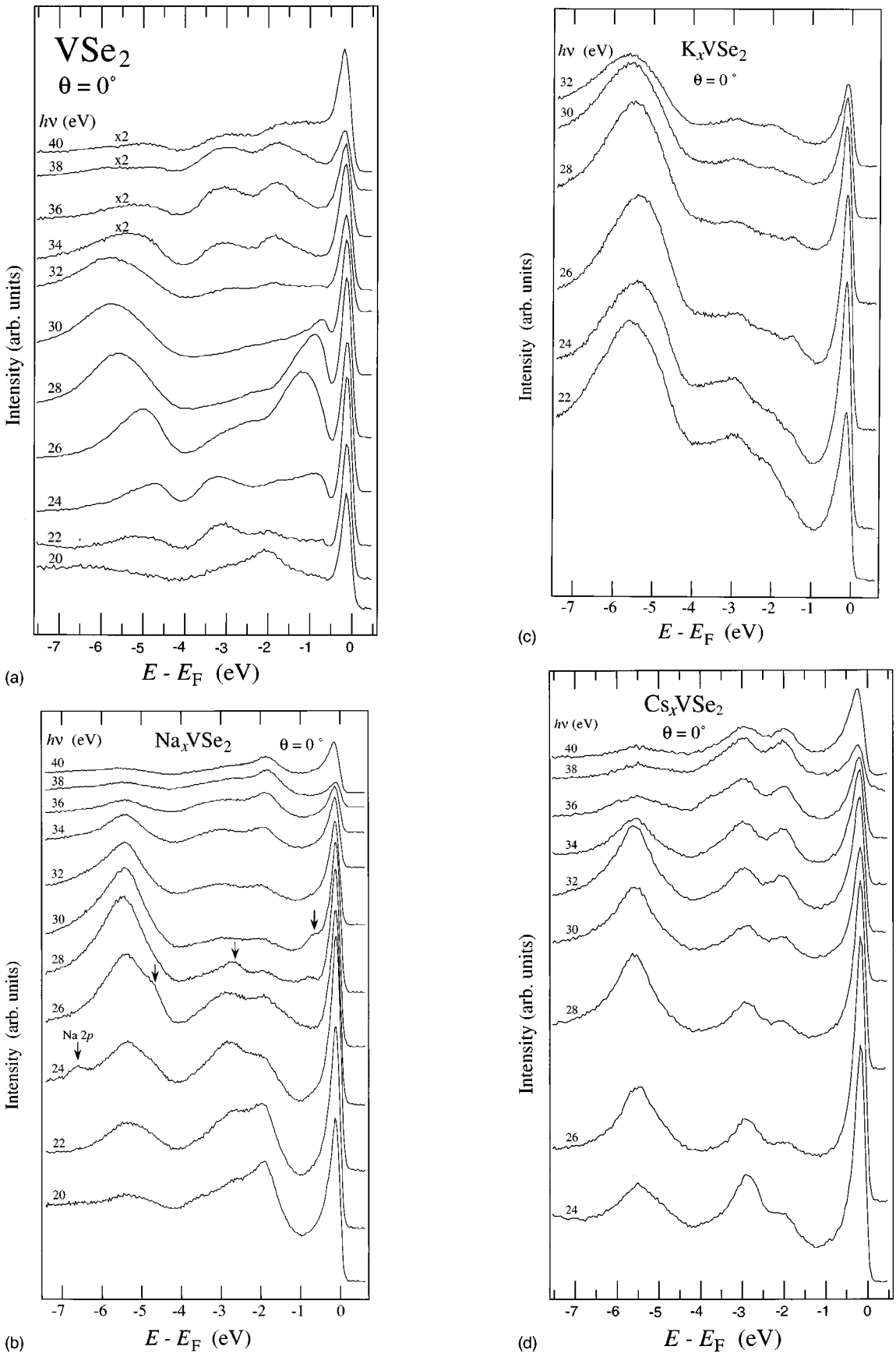

FIG. 6. Normal-emission EDCs of (a) VSe_2 with $h\nu = 20-40$ eV, (b) Na_xVSe_2 with $h\nu = 20-40$ eV (arrows mark the Na $2p$ core level excited through second-order grating diffraction), (c) K_xVSe_2 with $h\nu = 22-32$ eV, and (d) Cs_xVSe_2 with $h\nu = 24-40$ eV.

TABLE II. Experimental band-structure characteristics of pure and alkali-metal-intercalated VSe_2. All entries are binding energies (relative to E_F) in eV. Entries are as in Table I, except that the symmetry points refer to the surface Brillouin zone.

		VSe_2	Na_xVSe_2	K_xVSe_2	Cs_xVSe_2
V 3*d*	$\overline{M}$	0.5	0.4	0.3	0.5
Se 4*p*	$\overline{\Gamma}$	0/5.7	---/5.4	---/5.3	---/5.5
	$\overline{M}$	1.2/6.0	1.7/5.6	2.0/5.3	1.6/5.7
	$\overline{K}$	2.7/4.9	2.9/5.2	2.9/5.2	3.0/4.9
Se 4*s*		13.0/15.1	---	---	---/15

whether such slow stacking transformations may contribute to the observed surface alkali core level shifts.

The spectra in Fig. 4 indicate that VSe_2 is intercalated with Na or Cs much more easily than with K. Already from the beginning the Na and Cs core-level spectra are dominated by the intercalation peaks, without drastic changes after additional depositions. Apparently, the composition in the near-surface region did not change much after the initial depositions. Further depositions seem to mainly increase the intercalation depth. Contrary to this behavior, a much larger part of the deposited K remained at the surface and the intercalation rate was lower. Several depositions were required before the intercalation peak became comparable in intensity to the surface peak. Furthermore, the K depositions were accompanied by large increases in the inelastic background of the valence band spectra [see Fig. 6(c)], which indicates an accumulation of disordered K species on the surface. The different alkali intercalation tendencies are not due to simple size effects either, as Cs intercalates about as easily as Na. The lower intercalation rate of K is possibly due to the intercalation compound being less stable than for Na or Cs, but it may also be due to larger stability of the K surface species. In particular, if a relatively stable K overlayer is formed, with low sticking probability for additional K at room temperature, this may act as a shield against further K adsorption and intercalation.

Our observations of K being less prone to intercalate was further corroborated by Na/K codeposition experiments, which are reported in greater detail elsewhere.[27] When Na was deposited onto VSe_2 already intercalated with K an exchange reaction was observed, with Na replacing most of the intercalated K, which returned to the surface.

Writing the chemical composition after intercalation as A_xVSe_2 (A=Na, K, or Cs), one may estimate the alkali-metal concentration x from the relative spectral intensities of the Na 2*p*, K 3*p*, and Cs 4*d* levels as compared to the Se 3*d* level, using calculated atomic photoionization cross sections.[48] Generally, x seems to saturate at 0.2–0.3 after repeated depositions. For Na and Cs the saturation concentration was reached quickly, but for K it was reached more slowly. It should be pointed out that accurate determination of x from core-level intensities is extremely complicated due to the uneven depth distribution of the various elements, with the first intercalated alkali-metal layer being buried under a full VSe_2 sandwich. Therefore, the numbers given here are not to be taken too literally. However, seen as lower limits, the estimated concentrations appear reasonable, and the saturation tendency, seen for all three alkali metals, is striking. It seems that a migration to a larger intercalation depth is energetically favorred as the saturation concentration is approached. Studies of other *in situ* intercalation systems have yielded a variety of stoichiometries: $Na_{0.1}WSe_2$ (Ref. 11), $Na_{0.3}TaS_2$ (Ref. 18), $K_{0.5}WS_2$ (Ref. 9), $Cs_{0.6}TaSe_2$ (Ref. 13), and $Cs_{0.2}ZrSe_2$ (Ref. 21).

Analogous estimates of the number of surface alkali-metal atoms per formula unit of the first VSe_2 host layer suggest a significantly larger value for K (0.2–0.3) than for Na ($<$0.1) or Cs (0.1–0.2). Surface contamination may strongly influence both the the adsorption of deposited alkali metals, and its subsequent intercalation or trapping at the surface. The clean VSe_2 surface is extremely inert, but one may imagine that the reactivity of the surface should increase drastically after alkali-metal deposition. However, neither in core-level nor in valence-band spectra have we observed significant contamination induced features within the timespan of the measurements, except possibly for K deposition which caused a large increase in the valence-band inelastic background. However, this latter background increase is primarily an indication of surface disorder, which does not necessarily involve contamination. So, although surface contamination will eventually occur and affect the surface chemistry of any alkali/TMDC systems, we have not found evidence for contamination being the primary cause of the observed time dependence of the surface alkali core levels.

B. Core-level screening

Apart from information about the chemical state of a certain element through the appearance of chemically shifted components, the line shape of individual core-level peaks carries information about the local screening of the corresponding core holes. For metallic systems the screening by the conduction electrons gives rise to many-electron excitations within the conduction band, which results in asymmetric lineshapes with a characteristic tail on the high-BE side of the peak.[49–51] Through the screening by low-energy excitations, the line shape becomes strongly dependent on the density of states close to the Fermi level.[52] Core-level line shapes of metallic TMDC's have been successfully modeled by taking into account the conduction electron screening response and the finite core-hole lifetime.[53–56] It is clear from Fig. 4 that, in addition to its 0.8-eV spin-orbit splitting, the Se 3*d* line shape is asymmetric with a characteristic ''metallic'' tail already for pure VSe_2, and the line shape becomes even more asymmetric as the sample is intercalated with Na. This is contrary to what one would expect from the RBM: As more electrons are transferred to the initially half-filled lowest V 3*d* band, the reduced number of unoccupied states available just above the Fermi level should lead to reduced metallic screening. The failure of the RBM in the present

case is not unexpected, however, as according to the LAPW calculations intercalation with Na, K, or Cs should result in three partially filled bands taking part in the screening process, instead of only one.

The full width at half maximum of the Se $3d_{5/2}$ level was increased from 0.6 to 0.7 eV by the initial Na deposition, but was not changed significantly by the additional depositions. Most of this broadening is probably part of the screening induced line-shape changes, possibly with some additional broadening due to random variations in the coordination of Se atoms by Na. The BE of the Se $3d_{5/2}$ level was initially 53.3 eV, with an increase by about 80 meV observed directly after the initial Na deposition. With time, the shift was reversed, and 6.5 h later the peak appeared with about 45-meV lower BE than for pure VSe_2. After 13 h the $3d_{5/2}$ peak had returned to its initial BE, and a second Na deposition caused no change. This peculiar behavior can be analysed in terms of two different contributions: (i) intercalation-induced changes of the electronic structure, including the concentration dependent amount of charge transferred to the host layers; and (ii) the local effect on the first host layer of surface alkali species, which may also include some charge transfer. As the concentration of intercalated alkali metals and the nature of the surface species are both time dependent, the combined effect is rather complex.

C. Agreement with calculations

Before comparing with the experimental results, it is worth considering the band-structure changes upon alkali intercalation as predicted by the LAPW calculations. For all three compounds the valence-band maximum is located at Γ, but the conduction-band minimum, which is found at L for VSe_2, behaves differently. It remains at L for $NaVSe_2$, but is found at M for both $KVSe_2$ and $CsVSe_2$. Similarly, the valence-band minimum is found at Γ for $NaVSe_2$ (as in VSe_2), but at M for $KVSe_2$ and $CsVSe_2$. Furthermore, the calculations predict a small direct p/d overlap at Γ for $KVSe_2$, but small p/d gaps for both $NaVSe_2$ and $CsVSe_2$. This may indicate a difference in the alkali/host hybridization, which is possibly connected with the lower intercalation tendency of K, but without further calculations this remains highly speculative. Thus, with the exception of the perpendicular dispersion (discussed in Sec. IV D), there is no obvious dependence of the band-structure characteristics on the size of the intercalated alkali. In this context one may consider the hybridization of the host bands with unoccupied alkali-metal states. In addition to the similar alkali s states, there are also Na $3p$ states, K $3d$ states, and Cs $4f$ states, respectively, which should interact very differently with the occupied states. This may contribute significantly to the differences between $NaVSe_2$, $KVSe_2$, and $CsVSe_2$.

Normal-emission EDCs reflect the band structure along the ΓA line in **k** space, and the dispersion of some features, as $h\nu$ is varied, which is clearly seen in Fig. 6(a), proves that several bands of pure VSe_2 are dispersive also perpendicular to the layers. To compare this perpendicular band dispersion with the calculated bands, we need to find the perpendicular wave-vector component $k_\perp$ for each direct transition. To do this accurately requires that the final-state bands are known, however. In many cases, a satisfactory analysis is possible by approximating the final-state bands with a free-electron parabola, shifted by a suitable inner potential: $E_f=\hbar^2k^2/2m+V_0$. Although such an approach produced partial agreement between our LAPW bands and VSe_2 normal-emission data in a previous study,[19] serious discrepancies remained due to the very complicated nature of the VSe_2 upper bands. However, exactly those upper bands needed for proper mapping of the perpendicular dispersion can be determined by very-low-energy electron diffraction (VLEED) measurements.[57] In a recent study,[58] we applied this technique to VSe_2 as a supplement to normal-emission PES, and found excellent agreement between the experimental data and the LAPW bands along ΓA, except that the flat band $\sim$2 eV below E_F was placed $\sim$0.3 eV too low by the LAPW calculation, and that the dispersive band minimum at A, $\sim$3 eV below E_F, was placed $\sim$0.1 eV too high.

For the PES data obtained with variable emission angle θ, the parallel wave vector of each observed transition can be determined as $k_\parallel=0.512\sqrt{E_k}\,\sin\theta$ (with $k_\parallel$ and E_k in units of Å^{-1} and eV).[59] Direct comparison with the LAPW bands is now possible, by means of structure plots showing the initial state energy for each spectral peak as a function of $k_\parallel$ along a relevant azimuthal direction. The structure plots representing our angular series of EDCs for VSe_2 are shown in Fig. 7, for Na_xVSe_2 in Fig. 8, for K_xVSe_2 in Fig. 9, and for Cs_xVSe_2 in Fig. 10. As the perpendicular wave-vector component $k_\perp$ is undetermined, we compare our experimental points with the LAPW bands corresponding to the symmetry planes with $k_\perp=0$ (ΓMK plane of the BZ, full lines), and $k_\perp=\pi/c$ (ALH plane of the BZ, dashed lines). For each line in **k** space with constant $k_\parallel$, the minimum and maximum energies of each band are with few exceptions, found at the intersection with these planes, and so the experimental points of Figs. 7–10, which appear in the shaded areas between associated bands, are also consistent with the calculations. To be strict, the experimental points should be compared to the surface projected band structure, but the shaded areas constitute a close approximation. Filled and open symbols indicate conspicious and weak spectral peaks, respectively. In Figs. 7(a), 7(b), and 10(b), symbols of different shapes are used to distinguish between results obtained with different values of $h\nu$, as the involved transitions will differ in terms of $k_\perp$. In Fig. 8(b), symbols of different shape indicate whether the results were obtained after one or two Na depositions.

For VSe_2, the agreement between experiment and calculation is generally very good, and most spectral features can be readily identified. Figure 7(a) shows the structure plot for the $\bar{\Gamma}\bar{K}$ azimuth compared with the LAPW bands along ΓKM and AHL, and Fig. 7(b) the structure plot for the $\bar{\Gamma}\bar{M}$ and $\bar{\Gamma}\bar{M}'$ azimuths compared with the ΓM and AL bands. It should be noted that although the bands in the $\bar{\Gamma}\bar{M}$ and $\bar{\Gamma}\bar{M}'$ directions look the same, peak intensities could change drastically due to matrix element effects, and excitations may switch between different final bands when changing between the two different directions.

A spectral feature could therefore be weak or invisible when measuring in the $\bar{\Gamma}\bar{M}$ direction, but clearly observable in $\bar{\Gamma}\bar{M}'$ (or vice versa), and if a peak associated with a certain initial band appear to shift when going from one azimuth to the other, this may indicate a change to a different

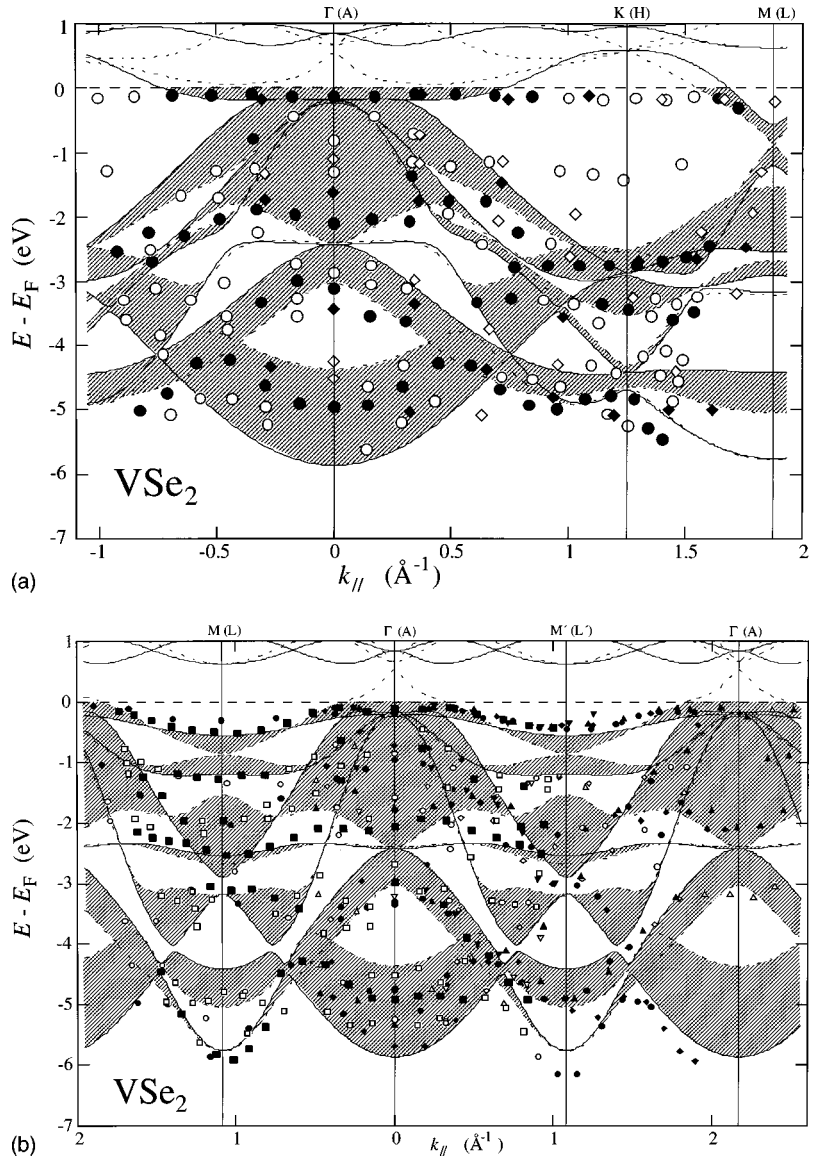

FIG. 7. Structure plots for VSe_2 along the (a) $\bar{\Gamma}\,\bar{K}$ and (b) $\bar{\Gamma}\,\bar{M}$ directions. Filled symbols correspond to conspicous spectral peaks, open symbols to weaker structures. The experimental data in (a) were obtained with (○) $h\nu=21.22$ eV and (◇) $h\nu=24$ eV; in (b) with (▽) $h\nu=14$ eV, (□) $h\nu=21.22$ eV, (○) $h\nu=24$ eV, (◇) $h\nu=30$ eV, and (△) $h\nu=38$ eV. Comparisons are made with the VSe_2 LAPW bands calculated along (a) ΓKM (full lines) and *AHL* (dashed lines), and (b) ΓM (full lines) and *AL* (dashed lines).

final band (and different $k_\perp$). Despite the overall agreement, some deviations are found. In Fig. 7(a) two weak experimental structures without corresponding LAPW bands are seen around $\bar{K}$. The first one, just below E_F, can be explained by indirect transitions from the occupied portions of the lowest V $3d$ band, which crosses E_F at $k_\parallel \approx 0.7$ Å^{-1} to emerge again halfway between $\bar{K}$ and $\bar{M}$. Also, the other feature, about 1.3 eV below E_F, is probably due to inelastic transitions, although their origin is less clear. As listed in Table II, the minimum of the half-filled V $3d$ band is found 0.5 eV below E_F, at $\bar{M}$, i.e., the observed occupied bandwidth is 0.5 eV. Due to the Fermi-Dirac cutoff, the V $3d$ peak becomes distorted near E_F, however, and is never seen to reach E_F. As a consequence, the apparent dispersion of the V $3d$ peak is only 0.4 eV. The value of 0.3 eV, reported in Ref. 30, is actually the apparent dispersion, while the minimum reported was also about 0.5 eV below E_F. Thus, the occupied V $3d$ width is larger than reported before, but still significantly smaller than the calculated occupied width of 0.8 eV. It should be noted, however, that the calculations place the minimum of this band at L, while at M the band is only 0.6 eV below E_F, in better agreement with the experimental dispersion. Actually, apart from being about 0.1 eV higher in energy, the experimental points follow the LAPW band along $\Gamma M(\Gamma M')$ fairly well. Close to the zone center, however, complications arise due to overlap with Se $4p$ bands.[30] There is an apparent discrepancy in Fig. 7(b) between the experimental points for the lowest Se $4p$ band around $\bar{M}$ and $\bar{M}'$, in that the points around $\bar{M}'$ fall almost 0.4 eV below the calculated band. As the perpendicular dispersion of the band is virtually zero here, this is not an effect of different final bands. Rather, the discrepancy is due to the corresponding EDC peaks being too broad (through lifetime broadening) to allow for accurate determination of their BE.

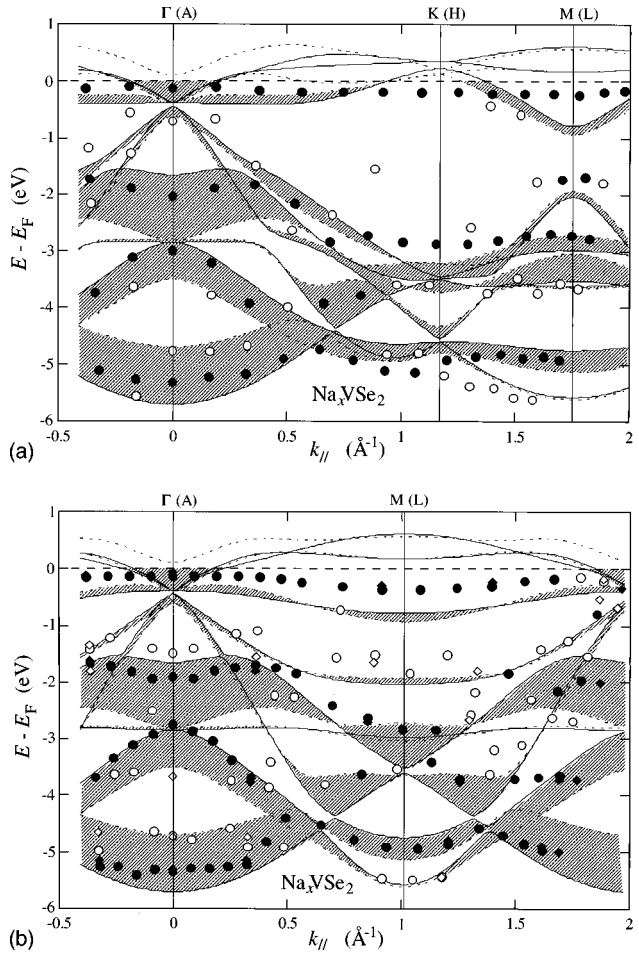

FIG. 8. Structure plots for Na_xVSe_2 along the (a) $\bar{\Gamma}\,\bar{K}$ and (b) $\bar{\Gamma}\,\bar{M}$ directions. Filled symbols correspond to conspicous spectral peaks, open symbols to weaker structures. The circles (diamonds) in the $\bar{\Gamma}\,\bar{M}$ direction refer to experimental data after one (two) Na depositions. The experimental data were obtained with $h\nu = 24$ eV. Comparisons are made with the $NaVSe_2$ LAPW bands along (a) ΓKM (full lines) and *AHL* (dashed lines), and (b) ΓM (full lines) and *AL* (dashed lines).

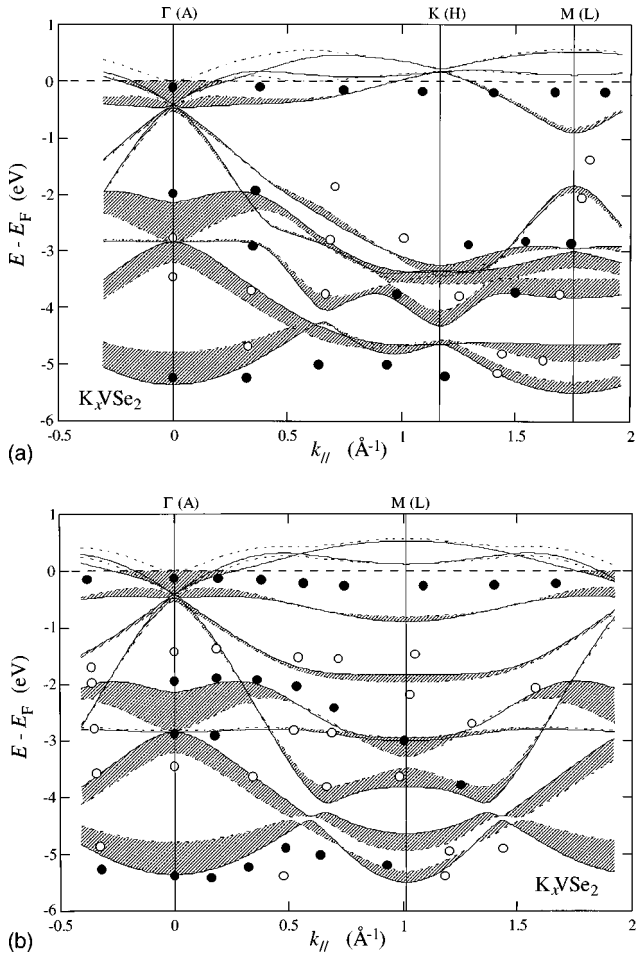

FIG. 9. Structure plots for K_xVSe_2 along the (a) $\bar{\Gamma}\,\bar{K}$ and (b) $\bar{\Gamma}\,\bar{M}$ directions. Filled symbols correspond to conspicous spectral peaks, open to weaker structures. The experimental data were obtained with $h\nu = 24$ eV. Comparisons are made with the $KVSe_2$ LAPW bands along (a) ΓKM (full lines) and *AHL* (dashed lines), and (b) ΓM (full lines) and *AL* (dashed lines).

Regarding the flat band about 2 eV below E_F around $\bar{\Gamma}$, the experimental points in both Figs. 7(a) and 7(b) place this band about 0.3 eV higher than calculated, in agreement with the recent PES/VLEED study.[58]

The agreement between experimental points and calculated bands, in different azimuthal directions, is also striking after intercalation with alkali metals, as can be seen in Figs. 8–10. From the core-level spectra, a concentration $x \approx 0.25$ was estimated for all compounds. The near-surface region appear to be rather homogeneously intercalated, and the intercalation induced changes are obviously well developed. The EDC's from K_xVSe_2 have high inelastic background levels, but the agreement between experimental points and LAPW bands is still notable. A common feature of all three compounds is that the observed dispersion of the lowest V $3d$ band (just below E_F) is much smaller (0.1–0.2 eV) than calculated. One must remember here, however, that the apparent dispersion is reduced by the Fermi-Dirac cutoff, and that the calculations were made for the fully intercalated compounds, while the measurements were done on compounds with less occupied V $3d$ bands. Another discrepancy is that the V $3d$ peak is visible in the vicinity of $\bar{K}$, despite the fact that the band here should be above E_F. The V $3d$ electrons are known to become localized in Li_2VSe_2 and in Na_xVSe_2 for $x > 0.6$ (Ref. 3), but the fact that some dispersion is still seen, and that the peak show a pronounced loss of intensity close to where the calculated band crosses E_F on approaching $\bar{K}$, indicates that the band picture still is valid. The remaining intensity at $\bar{K}$ can be attributed to indirect transitions, or due to energy broadening of the band, resulting in a tail below E_F even at $\bar{K}$. The LAPW calculations also predict additional V $3d$ bands to reach below E_F around $\bar{\Gamma}$, but we were not able to observe them directly. However, the increased Se $3d$ line-shape asymmetry, commented upon in Sec. IV B, might be a consequence of these bands being populated. The weak features observed at $\bar{\Gamma}$ (4-eV BE) and $\bar{K}$ (1.6-eV BE) for Cs_xVSe_2 are probably also due to indirect transitions from critical points with high density of states, and also for the other compounds some weak features may be due to indirect transitions.

In addition to the results shown in Fig. 2, the LAPW calculations also yielded two dispersive bands of Se $4s$ char-

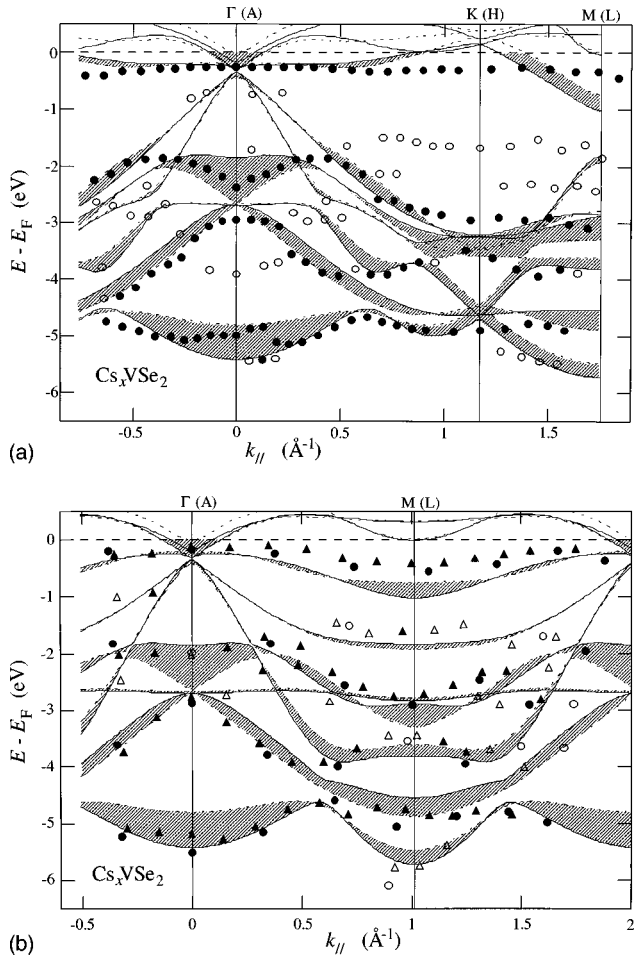

FIG. 10. Structure plots for Cs_xVSe_2 along the (a) $\bar{\Gamma}\,\bar{K}$ and (b) ΓM directions. Filled symbols correspond to conspicous spectral peaks, open to weaker structures. The experimental data in (a) were obtained with $h\nu = 21.22$ eV; in (b) with (○) $h\nu = 24$ eV, and (△) $h\nu = 21.22$ eV. Comparisons are made with the $CsVSe_2$ LAPW bands along (a) ΓKM (full lines) and *AHL* (dashed lines), and (b) ΓM (full lines) and *AL* (dashed lines).

acter. The calculated BE range of these bands was 12.5–14.7 eV for pure VSe_2, and slightly narrower (12.9–14.5 eV) for $CsVSe_2$. A curious effect of the Cs intercalation is that the Se 4*s* band dispersions along ΓA are reversed. This is most likely caused by the additional minima in the perpendicular periodic potential introduced by the alkali-metal layers. The CFS spectra (*i*) and (*ii*) in Fig. 5(a), corresponding to $\bar{\Gamma}$ and $\bar{M}$, respectively, show two peaks and one shoulder in the BE range 13.0–15.1 eV for VSe_2. The LAPW bands along ΓM (and *AL*) are shown as an inset in Fig. 5(a), on a common energy scale. Two peaks, with Be's of 13.9 and 15.1 eV are experimentally observed at normal emission (corresponding to $\bar{\Gamma}$), with an additional shoulder at 13.0-eV BE. In the spectrum corresponding to the $\bar{M}$ point the peak at 15.1-eV BE remains, while the other peak is shifted to 13.3-eV BE. However, this shift may not be due to true dispersion, as it could be just an effect of the shoulder becoming more prominent. Despite being rather core-level-like, the experimental width of the Se 4*s* ''band'' is in fairly good agreement with the LAPW width, and the measured average BE is only 0.5 eV higher than predicted. Despite overlap with the Cs 5*p* states and the above-mentioned ispersion reversal, it is also clear from Fig. 5(a) that the visible effect on the Se 4*s* states of the Cs deposition is small.

Figure 5(b) shows Cs 5*p* spectra measured in both CFS and EDC modes from Cs_xVSe_2. In analogy with the Cs 4*d* levels one finds separate $5p_{3/2}$ and $5p_{1/2}$ features, each split further into surface and intercalation components. The intercalation peaks have BE's of 10.4 and 12.0 eV. The LAPW calculations resulted in three dispersive Cs 5*p* bands in the BE range 9.6–12.3 eV, but detailed comparisons are not meaningful, since the calculations neglected the spin-orbit splitting. Considering the complications posed by Fermi-level distortion, incomplete intercalation, lifetime broadening of Se 4*p* bands, and the effects of perpendicular dispersion, the experimental band-structure characteristics collected in Table II still compares very favorably with its calculated counterparts in Table I.

D. Reduced dimensionality

Generally, intercalation of TMDC's with alkali metals increases the spacing between the host layers, which reduces the direct electronic overlap between the layers, and hence the perpendicular dispersion. This is in strong contrast to TMDC's intercalated with 3*d* transition metals, where strong hybridization between host valence states and intercalant 3*d* states strengthens the interlayer bonding.[2,3] The alkali-induced changes in the interlayer coupling are clearly manifested in the calculated LAPW bands of Fig. 2: For VSe_2, two bands below E_F, presumably of Se $4p_z$ character, are seen to have strong dispersion along the ΓA symmetry line. The upper one of these has a width of 2.8 eV, but on intercalation with Na, K, and Cs the width is reduced to 1.8, 1.2, and 0.8 eV, respectively. Similarly, the width of the lowest band is reduced from 1.5 eV, to 1.1, 0.6, and 0.6 eV, respectively. The calculated perpendicular dispersion over the entire BZ is discernible in Figs. 7–10 as the vertical widths of the shaded areas. Also, some earlier calculations for intercalated TMDCs predicted reduced perpendicular dispersion.[21,22,24,60–63]

The measured EDC's of pure VSe_2 are characterized by dispersive spectral features in directions both perpendicular and parallel to the layers [see Figs. 6(a), 7(a), and 7(b)], which clearly shows that the valence band is of 3D character. Although the analysis of normal emission EDC's in terms of perpendicular dispersion is complicated, our recent study[58] involving VLEED measurements shows that the PES results are in good agreement also with the calculated perpendicular dispersion for VSe_2.

The most striking effect on of the alkali intercalation seen in PES is the great reduction of peak dispersion in the measured normal emission EDC's [Fig. 6(b)–6(d)]. For Na_xVSe_2 some small dispersion remains (at most 0.3 eV for the upper dispersive band, which is almost a factor of 6 less than calculated), possibly also for K_xVSe_2, but for Cs_xVSe_2 no dispersion at all is found within the experimental accuracy. This may be interpreted as a transition from 3D to 2D character of the valence band, caused by intercalation-induced decoupling of the VSe_2 layers, but the effect is very much stronger than predicted by the LAPW calculations. This is a serious discrepancy, particularly so when considering the good

agreement found for the parallel dispersion. The explanation may fall into two different categories: either the perpendicular dispersion is really reduced much more than predicted, or otherwise the sensitivity of the PES experiment to the perpendicular dispersion is somehow lost for the intercalated samples.

If the perpendicular dispersion after intercalation really is much less than calculated, one straightforward explanation would be that the interlayer separation is larger than assumed in the calculations. This explanation is contradicted, however, by the good agreement found between the experimental and calculated parallel dispersions, which are also sensitive to the interlayer separation. Other explanations may involve correlation effects which could cause localization on the layers as the interlayer overlap is reduced below some critical limit, but without improved theoretical modeling and further experimental evidence this remains highly speculative.

The other possibility to consider, that the valence bands still have perpendicular dispersion after intercalation, but that normal-emission EDC's becomes insensitive, is to some extent supported by some features in the experimental structure plots (Figs. 8–10): Consider the two spectral features that are observed for Na_xVSe_2 at $\bar{\Gamma}$ with a BE around 5 eV. The stronger feature has about a 0.6-eV-higher BE than the weaker feature, but both peaks appear in the energy range spanned by the lower dispersive ΓA band. It can be argued that both peaks originate from that band, as no other states should contribute. With similar arguments one can assign about 0.6- and 0.5-eV dispersions to the corresponding ΓA bands of K_xVSe_2 and Cs_xVSe_2, respectively, although the lower quality of the K_xVSe_2 surface requires some caution. The multiple peaks seen between 1.5- and 3.0-eV BE for all three intercalation compounds indicate even larger remaining perpendicular dispersion, but the presence of more than one band in this energy range makes the interpretation more uncertain. Nonetheless, considering these indications seen in the angular structure plots, it appears likely that the perpendicular band dispersions are close to the calculated results also for the intercalated samples. In order to explain why the perpendicular dispersions are not seen in the normal-emission EDC's, one may recall that the **k** conservation in the photoemission process depends on the translational symmetry of the sample.[64] The almost perfect periodicity along the surface of a well-prepared sample leads to rather strict conservation of $\mathbf{k}_\parallel$ (in a reduced zone scheme), but in the perpendicular direction one has to consider the very limited mean free path of the photoelectrons. With only the few uppermost layers contributing to the photocurrent, the $k_\perp$ conservation is significantly relaxed, and as a consequence the $h\nu$-dependent dispersion of direct transition peaks (in normal-emission EDC's) becomes less visible, and nondispersive structures reflecting the one-dimensional density of states along rods of constant $\mathbf{k}_\parallel$ may appear. Apparently, for the case of pure VSe_2 there is sufficient $k_\perp$ conservation for the perpendicular dispersion to be clearly visible, but not for the intercalated samples. Several circumstances may contribute to this: There is less dispersion to be seen in the intercalates, and simultaneously the $k_\perp$ conservation is further weakened by increased interlayer distance (and possibly decreased escape depth). Another reason, perhaps the most prominent one, for breakdown of the $k_\perp$ conservation, could be stacking disorder, induced by the $1T \rightarrow 3R$ structural changes mentioned previously. In the $1T \rightarrow 3R$ transformation the symmetry of the primitive unit cell is changed from hexagonal to rhombohedral, but it still contains the same number of atoms, and the hexagonal surface BZ is unchanged, so the band structure should be very similar, except possibly near certain symmetry points. If the transformation in large crystals is partially inhibited by inhomogeneous intercalation or by defects pinning the sandwiches together, this may well result in stacking disorder.

E. Charge transfer and the RBM

It was pointed out already in Sec. I that, strictly speaking, the RBM is unlikely to describe the intercalation induced changes in the electronic structure accurately. This assumption is accentuated by the calculated LAPW bands, and clearly verified by the experimental results. The strongly increased anisotropy upon intercalation is not predicted by the RBM, and other significant changes, incompatible with the RBM, are found also in the mapping of bands parallel to the layers.

The charge transfer from alkali metals to host layers is complete in the sense that, after intercalation, the valence electrons provided by the alkali metals are found to occupy V $3d$ bands associated with host layers, rather than alkali-metal-derived bands. Due to hybridization between alkali metal and host layer bands, one should expect these occupied bands to have at least some small fraction of alkali-metal s character mixed into them, which would still leave some of the charge on the alkali metal ions. Whether the ionization of the alkali metal is complete or not, is therefore largely a matter of semantics.

Although there are notable changes in the details of the band structure upon intercalation, as well as hybridization between host and intercalant, the RBM admittedly describes essential aspects of the intercalation in a conceptually simple way, which is why it may still be used as a first approximation. Under conditions that band widths and energy gaps are not greatly affected, the RBM is particularly useful if the electronic bands are represented by their density of states only.[16]

Another observation is that most of the RBM incompatible changes seem to occur at a very early stage of the intercalation. This is reflected by the striking agreement between our LAPW calculations, assuming fully intercalated samples, and our experimental results obtained with alkali-metal concentrations estimated to be only $\sim$25% of that. It seems that the layer decoupling, and the associated major electronic structure modifications, take place immediately after the onset of intercalation, and that the effects of continued intercalation are relatively well described by application of the RBM on the modified band structure.

VI. CONCLUSIONS

The electronic structure of pure and alkali-metal-intercalated VSe_2 has been studied using angle-resolved photoemission. Na and Cs easily intercalate VSe_2, while K intercalates at a markedly lower rate. The concentration of intercalated alkali metals appeared to reach some kind of equilibrium at about 0.25 alkali atoms per VSe_2 formula unit,

with diffusion to larger depths favored at higher concentrations. The increased asymmetry of the Se 3*d* level after intercalation reflects changes in the conduction-band structure and a modified carrier density.

The valence bands of VSe_2 were found to be of 3D character, and in good agreement with the LAPW band calculations. *In situ* intercalation with Na, K, and Cs induced a transition from 3D to 2D character, which is largely explained by charge transfer to the host lattice and decoupling of the VSe_2 layers induced by the intercalated alkali ions. Also, after the intercalation good agreement was found between the experimental results and the LAPW band calculations, particularly in terms of band dispersion parallel to the layers, but the calculations do not fully support the 3D to 2D transition, as some perpendicular dispersion are still predicted. This discrepancy could be due to reduced $k_\perp$ resolution in normal-emission measurements, structural rearrangements with associated stacking disorder, or correlation effects which may weaken the interlayer coupling. The LAPW calculations show differences between $NaVSe_2$, $KVSe_2$, and $CsVSe_2$ which cannot be explained as alkali size effects.

The observed changes in both experiments and calculations are more extensive than predicted by the RBM, which should be used only as a first approximation. It is remarkable, however, that the major modifications of the band structure are well developed already at alkali concentrations far below those assumed in the LAPW calculations, which is why the effects of continued intercalation might be reasonably well described by the RBM, applied on the modified band structure.

Further studies are required to resolve the question of whether the *in situ* intercalation induces stacking disorder via incomplete structural transitions. In particular, there is a need for studies that probe both crystallographic and electronic structure, which are strongly interrelated. Structural changes occurring upon intercalation may create various kinds of defects, which in turn may have a strong influence on both the alkali-metal adsorbtion on the surface and the diffusion into the bulk, which is why it is essential that the defect structure and its influence on the *in situ* intercalation kinetics are investigated. A better understanding of the $k_\perp$ resolution (or lack of it) in angle-resolved PES from intercalated TMDC's is also desirable.

ACKNOWLEDGMENTS

This work was supported by the Swedish Natural Science Research Council. L. Ilver, J. Kanski, and P.-O. Nilsson are acknowledged for stimulating discussions. We also want to thank Professor F. Lévy for providing high-quality VSe_2 samples, and the staff at MAX-lab for their skillful assistance.

[1] J. A. Wilson and A. D. Yoffe, Adv. Phys. **18**, 193 (1969).
[2] W. Y. Liang, in *Intercalation in Layered Materials*, edited by M. S. Dresselhaus (Plenum, New York, 1986).
[3] R. H. Friend and A. D. Yoffe, Adv. Phys. **36**, 1 (1987).
[4] H. I. Starnberg, and H. P. Hughes, J. Phys. C **20**, 4429 (1987).
[5] W. Jaegermann, F. S. Ohuchi, and B. A. Parkinson, Surf. Sci. **201**, 211 (1988).
[6] W. Jaegermann, F. S. Ohuchi, and B. A. Parkinson, Surf. Interface Anal. **12**, 293 (1988).
[7] C. Pettenkofer, W. Jaegermann, and B. A. Parkinson, Surf. Sci. **251/252**, 583 (1991).
[8] A. Klein, J. Lehmann, C. Pettenkofer, W. Jaegermann, M. Lux-Steiner, and E. Bucher, Appl. Surf. Sci. **70/71**, 470 (1993).
[9] F. S. Ohuchi, W. Jaegermann, C. Pettenkofer, and B. A. Parkinson, Langmuir **5**, 439 (1989).
[10] A. Schellenberger, R. Schlaf, T. Mayer, E. Holub-Krappe, C. Pettenkofer, W. Jaegermann, U. A. Ditzinger, and H. Neddermeyer, Surf. Sci. **241**, L25 (1991).
[11] A. Schellenberger, R. Schlaf, C. Pettenkofer, and W. Jaegermann, Phys. Rev. B **45**, 3538 (1992).
[12] A. Schellenberger, C. Pettenkofer, W. Jaegermann, C. A. Papageorgopoulos, and M. Kamaratos, Ber. Bunsenges. Phys. Chem. **96**, 1755 (1992).
[13] C. Pettenkofer, W. Jaegermann, A. Schellenberger, E. Holub-Krappe, C. A. Papageorgopoulos, M. Kamaratos, and A. Papageorgopoulos, Solid State Commun. **84**, 921 (1992).
[14] C. A. Papageorgopoulos, M. Kamaratos, A. Papageorgopoulos, A. Schellenberger, E. Holub-Krappe, C. Pettenkofer, and W. Jaegermann, Surf. Sci. **275**, 314 (1992).
[15] H. I. Starnberg, H. E. Brauer, L. J. Holleboom, and H. P. Hughes, Phys. Rev. Lett. **70**, 3111 (1993).
[16] W. Jaegermann, C. Pettenkofer, A. Schellenberger, C. A. Papageorgopoulos, M. Kamaratos, D. Vlachos, and Y. Tomm, Chem. Phys. Lett. **221**, 441 (1994).
[17] A. Schellenberger, W. Jaegermann, C. Pettenkofer, M. Kamaratos, and C. A. Papageorgopoulos, Ber. Bunsenges. Phys. Chem. **98**, 833 (1994).
[18] C. Pettenkofer and W. Jaegermann, Phys. Rev. B **50**, 8816 (1994).
[19] H. I. Starnberg, H. E. Brauer, P. O. Nilsson, L. J. Holleboom, and H. P. Hughes, Mod. Phys. Lett. B **8**, 1261 (1994).
[20] C. A. Papageorgopoulos and W. Jaegermann, Surf. Sci. **338**, 83 (1995).
[21] H. E. Brauer, H. I. Starnberg, L. J. Holleboom, and H. P. Hughes, J. Phys. Condens. Matter **7**, 7741 (1995).
[22] H. E. Brauer, H. I. Starnberg, L. J. Holleboom, and H. P. Hughes, Surf. Sci. **331–333**, 419 (1995).
[23] S. D. Foulias, D. S. Vlachos, C. A. Papageorgopoulos, R. Yavor, C. Pettenkofer, and W. Jaegermann, Surf. Sci. **352–354**, 463 (1996).
[24] H. E. Brauer, H. I. Starnberg, L. J. Holleboom, and H. P. Hughes, Surf. Sci. **357/358**, 4345 (1996).
[25] H. I. Starnberg, H. E. Brauer, and H. P. Hughes, J. Phys. Condens. Matter **8**, 1229 (1996).
[26] H. E. Brauer, Inger Ekvall, H. Olin, H. I. Starnberg, Erik Wahlström, H. P. Hughes, and V. N. Strocov, Phys. Rev. B **55**, 10 022 (1997).
[27] H. I. Starnberg, H. E. Brauer, and H. P. Hughes, Surf. Sci. **377–379**, 828 (1997).
[28] H. I. Starnberg, H. E. Brauer, and V. N. Strocov, Surf. Sci. **384**, L785 (1997).

[29] H. P. Hughes, C. Webb, and P. M. Williams, J. Phys. C **13**, 1125 (1980).
[30] M. T. Johnson, H. I. Starnberg, and H. P. Hughes, J. Phys. C **19**, L451 (1986).
[31] R. Claessen, I. Schäfer, and M. Skibowski, J. Phys. Condens. Matter **2**, 10045 (1990).
[32] A. R. Law, P. T. Andrews, and H. P. Hughes, J. Phys. Condens. Matter **3**, 813 (1991).
[33] H. I. Starnberg, P. O. Nilsson, and H. P. Hughes, J. Phys. Condens. Matter **4**, 4075 (1992).
[34] H. I. Starnberg, L. Ilver, P. O. Nilsson, and H. P. Hughes, Phys. Rev. B **47**, 4714 (1993).
[35] A. M. Woolley and G. Wexler, J. Phys. C **10**, 2601 (1977).
[36] A. Zunger and A. J. Freeman, Phys. Rev. B **19**, 6001 (1979).
[37] H. W. Myron, Physica B **99**, 243 (1980).
[38] D. D. Koelling and B. N. Harmon, J. Phys. C **10**, 3107 (1977).
[39] D. M. Ceperley and B. J. Alder, Phys. Rev. Lett. **45**, 566 (1980).
[40] M. S. Whittingham, Prog. Solid State Chem. **12**, 41 (1978).
[41] N. W. Ashcroft and N. D. Mermin, *Solid State Physics* (Holt, Rinehart and Winston, New York, 1976), p. 385.
[42] For convenience we use the terminology ''valence bands'' for bands of chalcogen *p* character, and ''conduction bands'' for bands derived from the metal *d* levels throughout this paper, although this is strictly correct only for the semiconducting group-IV TMDC's.
[43] H. I. Starnberg, P. O. Nilsson, and H. P. Hughes, Surf. Sci. **287/288**, 627 (1993).
[44] A. le Blanc, M. Danot, L. Trichet, and J. Rouxel, Mater. Res. Bull. **9**, 191 (1974).
[45] J. Rouxel, Physica B **99**, 3 (1980).
[46] G. A. Wiegers, Physica B **99**, 151 (1980).
[47] E. Sandré, R. Brec, and J. Rouxel, J. Solid State Chem. **88**, 269 (1990).
[48] J. Yeh and I. Lindau, At. Data **32**, 1 (1985).
[49] P. Nozieres and C. T. De Dominics, Phys. Rev. **178**, 1097 (1969).
[50] S. Doniach and M. Sunjic, J. Phys. C **3**, 285 (1970).
[51] G. K. Wertheim and S. Hüfner, Phys. Rev. Lett. **35**, 53 (1975).
[52] G. K. Wertheim and L. R. Walker, J. Phys. F **6**, 2297 (1976).
[53] R. Eppinga, G. A. Sawatzky, C. Haas, and C. F. van Bruggen, J. Phys. C **9**, 3371 (1976).
[54] J. A. Scarfe and H. P. Hughes, J. Phys. Condens. Matter **1**, 6865 (1989).
[55] H. P. Hughes and J. A. Scarfe, Phys. Rev. Lett. **74**, 3069 (1995).
[56] H. P. Hughes and J. A. Scarfe, J. Phys. Condens. Matter **8**, 1421 (1996); **8**, 1439 (1996); **8**, 1457 (1996).
[57] V. N. Strocov, H. I. Starnberg, P. O. Nilsson, and L. J. Holleboom, J. Phys. Condens. Matter **8**, 7549 (1996).
[58] V. N. Strocov, H. I. Starnberg, P. O. Nilsson, H. E. Brauer, and L. J. Holleboom, Phys. Rev. Lett. **79**, 467 (1997).
[59] H. P. Hughes and W. Y. Liang, J. Phys. C **6**, 1684 (1973).
[60] J. V. McCanny, J. Phys. C **12**, 3263 (1979).
[61] C. Umrigar, D. E. Ellis, D. Wang, H. Krakauer, and M. Pasternak, Phys. Rev. B **26**, 4935 (1982).
[62] G. Y. Guo and W. Y. Liang, J. Phys. C **20**, 4315 (1987).
[63] J. Dijkstra, C. F. van Bruggen, and C. Haas, J. Phys. Condens. Matter **1**, 4297 (1989).
[64] P. J. Feibelman and D. E. Eastman, Phys. Rev. B **10**, 4932 (1974).